Plasmon switching: Observation of dynamic surface plasmon steering by selective mode excitation in a sub-wavelength slit

S. B. Raghunathan,[1] C. H. Gan,[2,3] T. van Dijk,[4] B. Ea Kim,[2] H. F. Schouten,[4] W. Ubachs,[4] P. Lalanne,[2,5] and T. D. Visser[1,4,*]

[1]*Dept. of Electrical Engineering, Delft University of Technology, Delft, The Netherlands*
[2]*Laboratoire Charles Fabry, Institut d'Optique, Univ Paris-Sud, CNRS, Campus Polytechnique RD 128, 91127 Palaiseau cedex, France*
[3]*Electronics and Photonics Department, A*STAR Institute of High Performance Computing, 138632, Singapore*
[4]*Dept. of Physics and Astronomy, VU University, Amsterdam, The Netherlands*
[5]*Laboratoire Photonique, Numerique et Nanosciences - LP2N, Univ. Bordeaux, Institut d'Optique, 351 Cours de la Liberation, Talence, France*

*t.d.visser@tudelft.nl

Abstract: We report a plasmon steering method that enables us to dynamically control the direction of surface plasmons generated by a two-mode slit in a thin metal film. By varying the phase between different coherent beams that are incident on the slit, individual waveguide modes are excited. Different linear combinations of the two modes lead to different diffracted fields at the exit of the slit. As a result, the direction in which surface plasmons are launched can be controlled. Experiments confirm that it is possible to distribute an approximately constant surface plasmon intensity in any desired proportion over the two launching directions. We also find that the anti-symmetric mode generates surface plasmons more efficiently than the fundamental symmetric mode.

OCIS codes: (240.6680) Surface plasmons; (260.1960) Diffraction theory; (240.3990) Micro-optical devices; (250.5403) Plasmonics; (310.2785) Guided wave applications; (310.2790) Guided waves.

References and links

1. H. Raether, *Surface Plasmons on Smooth and Rough Surfaces and on Gratings* (Springer, Berlin, 1988).
2. H. A. Atwater, "The promise of plasmonics," Scientific American **296**, 56–62 (2007.
3. T. W. Ebbesen, H. J. Lezec, H. F. Ghaemi, T. Thio, and P. A. Wolff, "Extraordinary optical transmission through subwavelength hole arrays," Nature (London) **391**, 667–669 (1998).
4. T. Thio, K. M. Pellerin, R. A. Linke, H. J. Lezec, and T. W. Ebbesen, "Enhanced light transmission through a single subwavelength aperture," Opt. Lett. **26**, 1972–1974 (2001).
5. B. Steinberger, A. Hohenau, H. Ditlbacher, F. R. Aussenegg, A. Leitner, and J. R. Krenn, "Dielectric stripes on gold as surface plasmon waveguides: Bends and directional couplers," Appl. Phys. Lett. **91**, 081111 (2007).
6. S. A. Maier, P. G. Kik, H. A. Atwater, S. Meltzer, E. Harel, B. E. Koel, and A. A. G. Requicha, "Local detection of electromagnetic energy transport below the diffraction limit in metal nanoparticle plasmon waveguides," Nature Materials **2**, 229–232 (2003).
7. Q. Gan, Y. Gao, and F. J. Bartoli, "Vertical plasmonic Mach-Zehnder interferometer for sensitive optical sensing," Opt. Express **17**, 20747–20755 (2009).

#167889 - $15.00 USD Received 3 May 2012; revised 11 Jun 2012; accepted 14 Jun 2012; published 22 Jun 2012

8. M.A. Noginov, G. Zhu, A.M. Belgrave, R. Bakker, V.M. Shalaev, E. Narimanov, S. Stout, E. Herz, T. Suteewong, and U. Wiesner, "Demonstration of a spaser-based nanolaser," Nature (London) **460**, 1110–1113 (2009).
9. J.S.Q. Liu, R.A. Pala, F. Afshinmanesh, W. Cai, and M.L. Brongersma, "A submicron plasmonic dichroic splitter," Nat. Commun. **2**:525 doi: 10.1038/ ncomms1537 (2011).
10. F. López-Tejeira, S. G. Rodrigo, L. Martín-Moreno, F. J. García-Vidal, E. Devaux, T. W. Ebbesen, J. R. Krenn, I. P. Radko, M. U. González, J. C. Weeber, and A. Dereux, "Efficient unidirectional nanoslit couplers for surface plasmons," Nat. Phys. **3**, 324–328 (2007).
11. Y. Wang, X. Zhang, H. Tang, K. Yang, Y. Wang, Y. Song, T. Wei, and C. H. Wang, "A tunable unidirectional surface plasmon polaritons source," Opt. Express **17**, 20457–20464 (2009).
12. X. Li, Q. Tan, B. Bai, and G. Jin, "Experimental demonstration of tunable directional excitation of surface plasmon polaritons with a subwavelength metallic double slit," Appl. Phys. Lett. **98**, 251109 (2011).
13. A. Baron, E. Devaux, J. C. Rodier, J. P. Hugonin, E. Rousseau, C. Genet, T. Ebbesen, and P. Lalanne, "Compact antenna for efficient and unidirectional launching and decoupling of surface plasmons," Nano Lett. **11**, 4207-4212 (2011).
14. M. Miyata and J. Takahara, "Excitation control of long-range surface plasmons by two incident beams," Opt. Express **20**, 9493–9500 (2012).
15. M. Besbes, J. P. Hugonin, P. Lalanne, S. van Haver, O. T. A. Janssen, A. M. Nugrowati, M. Xu, S. F. Pereira, H.P. Urbach, A. S. van de Nes, P. Bienstman, G. Granet, A. Moreau, S. Helfert, M. Sukharev, T. Seideman, F. I. Baida, B. Guizal, and D. Van Labeke, "Numerical analysis of a slit-groove diffraction problem," J. Eur. Opt. Soc. Rapid Publ. **2**, 07022 (2007).
16. P. Lalanne, J. P. Hugonin, H. Liu, and B. Wang, "A microscopic view of the electromagnetic properties of sub-λ metallic surfaces," Surf. Sci. Rep. **64**, 453–469 (2009).
17. E. D. Palik (ed.), *Handbook of Optical Constants of Solids* (Academic Press, San Diego, 1998).
18. H. Liu, P. Lalanne, X. Yang, and J. P. Hugonin "Surface plasmon generation by subwavelength isolated objects," IEEE J. Sel. Top. Quantum Electron. **14**, 1522–1529 (2008).
19. L. Verslegers, Z. Yu, P. B. Catrysse, and S. Fan, "Temporal coupled-mode theory for resonant apertures," J. Opt. Soc. Am. B **27**, 1947-1956 (2010).
20. C. F. Bohren and D. R. Huffman, *Absorption and Scattering of Light by Small Particles* (Wiley, New York, 1983).
21. J. A. Schuller and M. L. Brongersma, "General properties of dielectric optical antennas," Opt. Express **17**, 24084–24095 (2009).
22. P. Lalanne and J. P. Hugonin, "Interaction between optical nano-objects at metallo-dielectric interfaces," Nat. Phys. **2**, 551–556, (2006).
23. C. Vassallo, *Optical Waveguide Concepts* (Elsevier, Amsterdam, 1991).
24. F.J. García-Vidal, H. J. Lezec, T. W. Ebbesen, and L. Martín-Moreno, "Multiple paths to enhance optical transmission through a single subwavelength slit," Phys. Rev. Lett. **90**, 213901 (2003).
25. A. Degiron and T. W. Ebbesen, "Analysis of the transmission process through single apertures surrounded by periodic corrugations," Opt. Express **12**, 3694–3700 (2004).
26. K. Aydin, A. O. Cakmak, L. Sahin, Z. Li, F. Bilotti, L. Vegni, and E. Ozbay, "Split-ring-resonator-coupled enhanced transmission through a single subwavelength aperture," Phys. Rev. Lett. **102**, 013904 (2009).
27. K. F. MacDonald, Z. L. Sámson, M. I. Stockman, and N. I. Zheludev, "Ultrafast active plasmonics," Nat. Photonics **3**, 55–58 (2009).

1. Introduction

An electromagnetic field directed at the interface between a metal and a dielectric can cause the free electrons in the metal to oscillate at the same frequency as the field. Under the right conditions such a collective excitation of electrons, known as a surface plasmon (SP), will propagate along the interface, and can be converted back into a freely propagating field when it is scattered by a surface imperfection such as a ridge or a groove [1]. The wavelength of an SP is much smaller than the wavelength of the electromagnetic field by which it is generated. This suggests the possibility of ultra-compact "plasmonic" devices in which information-carrying electromagnetic fields generate SPs that are then processed before being turned back again into a free field [2]. Following the observation of plasmon-enhanced transmission through subwavelength-size hole arrays [3] and single subwavelength apertures [4] in metal plates, numerous research efforts to develop nanoscale plasmonic devices were triggered. Plasmonic couplers [5], waveguides [6], interferometers [7], lasers [8] and dichroic splitters [9] have already been realized. However, for the field of plasmonics to achieve its full potential, it is necessary to control the direction in which SPs are launched. Compact schemes for directional launching of SPs based

#167889 - $15.00 USD Received 3 May 2012; revised 11 Jun 2012; accepted 14 Jun 2012; published 22 Jun 2012

on geometries such as a nanoslit with a Bragg resonator [10], an asymmetrically illuminated single nanoslit [11] and pairs of nanoslits [12], and an optimized multi-groove coupler [13] have been proposed and implemented, with extinction ratios as high as 50. These schemes all rely on some static, built-in asymmetry that favors a particular direction of SP launching. To address the important aspect of flexible directional launching of SPs, an essential feature for any kind of integrated plasmonic circuitry, we present a generic approach to dynamically switch plasmons between two channels with a constant total intensity and with a nanoscale footprint.

2. Theory

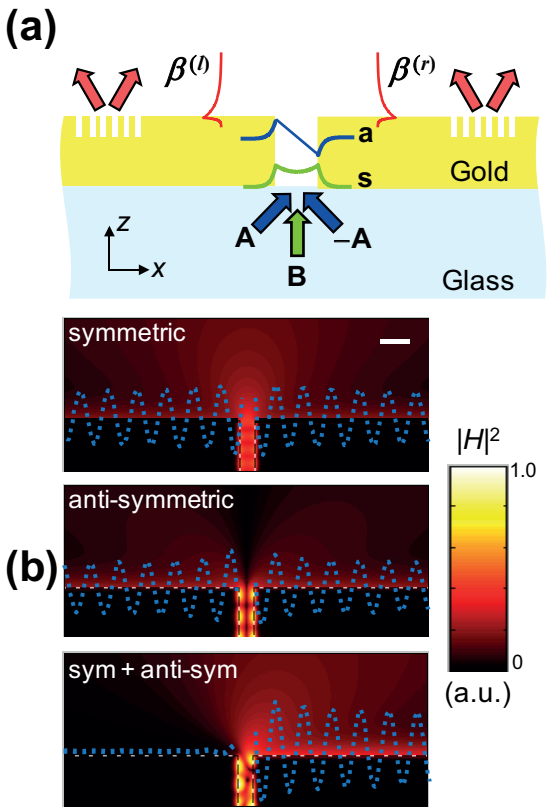

Fig. 1. Principle of the proposed surface plasmon steering method. (a) A subwavelength slit of width w in a gold film supports only two TM modes for $\lambda/2 \lesssim w \lesssim \lambda$: a symmetric mode (s, green curve) and an anti-symmetric mode (a, blue curve). Three coherent beams, A, -A (with opposite angle of incidence compared to A and π-phase shifted), and B are incident on the slit from the glass substrate. At the dark side of the film, SPs are launched to the left and to the right with amplitude $\beta^{(l)}$ and $\beta^{(r)}$, respectively. A series of grooves at 8 μm from either side of the slit converts the SPs back to freely propagating fields that are detected in the far field. (b) Illustrating how a coherent superposition of the a and s modes can lead to unidirectional SP launching at a gold-air interface. The first two panels show the intensity of the magnetic field when the slit is illuminated with either the s or the a mode. Superposed dotted blue curves show the total magnetic field scattered on the interface. The length of the white bar in the first panel indicates the illumination wavelength in vacuum ($\lambda = 600$ nm), and the slit width w is $\lambda/2$.

#167889 - $15.00 USD Received 3 May 2012; revised 11 Jun 2012; accepted 14 Jun 2012; published 22 Jun 2012

In its simplest form, our approach is depicted in Fig. 1(a), where a narrow slit in a thin gold film is illuminated from the glass substrate by three coherent beams with Transverse Magnetic (TM) polarization. The slit width is such that for an illumination wavelength λ only two TM modes–one symmetric (TM_0), the other anti-symmetric (TM_1)–are non-evanescent. Beam B is normally incident and therefore only excites the fundamental TM_0 mode. In the path of this beam a piezo element is mounted, allowing its phase to be varied. Beams A and $-$A, which have opposite but equal amplitudes, make an angle of $+\theta$ and $-\theta$ with B, respectively. They have the same intensity, but are $\pi-$phase shifted with respect to each other. It follows from symmetry that the combination of these two oblique beams excites only the TM_1 mode [14]. At the slit exit, both left and right travelling surface plasmons are generated. Their amplitudes are denoted by $\beta^{(l)}$ and $\beta^{(r)}$, respectively. A series of grooves on either side of the slit is used to evidence the steering effect by converting the launched plasmons back to freely propagating fields whose intensity is measured in the far field.

To illustrate how plasmon beam steering may be achieved with a two-mode nanoslit, Fig. 1(b) shows the interference pattern generated by an appropriate linear combination of the TM_0 and TM_1 modes in the slit. These modes scatter at the slit exit and a complete extinction of SPs in one launching direction is predicted. The fields are calculated with a frequency-domain, aperiodic Fourier modal method, incorporating perfectly-matched layers (method MM3 in the benchmark article Ref. [15]). The distributions of the magnetic field intensity $|H|^2$ in the near field of the metal-air interface are first shown for the cases where the same slit is illuminated with either the symmetric TM_0 or the anti-symmetric TM_1 mode. To illustrate the phase relationship between the excited SP fields, the total magnetic field $\mathrm{Re}(H)$ on the gold-air interface is superimposed as a dotted red curve. On each side, the oscillating wave is composed of an SP mode, and a quasi-cylindrical wave that rapidly decays within a few-wavelengths from the slit [16]. For illumination with either the TM_0 or the TM_1 mode, the fields on opposite sides of the slit are in phase or $\pi-$phase shifted, respectively. Let us adjust the (complex) amplitude of the TM_0 mode such that it excites SPs on the right side of the slit with the same phase and intensity as the TM_1 mode. It is apparent that the linear combination of the two modes (Fig. 1(b), right panel) then gives rise to complete destructive interference on the left side of the slit whereas constructive interference takes place on the right side. In the specific example of Fig. 1(b) it is taken that $\lambda = 600$ nm, $w = \lambda/2$, and the refractive index of gold $n_{\mathrm{Au}} = 0.23 + \mathrm{i}2.98$ (see Ref. [17]). The right-most panel of Fig. 1(b) clearly shows that the total field at the gold-air interface is almost null to the left of the slit, indicating that not only the SP excitation is zero, but also that the excitation of the accompanying quasi-cylindrical waves is very weak.

As explained, beams A and -A together excite only the TM_1 mode whereas beam B excites only the TM_0 mode. At the slit exit, each mode can be scattered into radiation that propagates to the far field, or can be dissipated as absorption loss on the gold surface, or be reflected as a backward propagating mode in the slit. Part of the absorption loss is carried by the SPs launched on both sides of the slit. Let the SP scattering coefficients at the left- and right-hand side of the slit for the two-beam system $\{\mathrm{A}, -\mathrm{A}\}$ be A_a and $-A_a$, respectively. For beam B we denote the SP scattering coefficient on each side by B_s. To calculate these coefficients, we use the mode orthogonality of translational-invariant lossy waveguides [16], which yields $A_a = \int_{-\infty}^{\infty} [E_z^{(a)}(x,z) H^{\mathrm{SP}}(x,z) - H^{(a)}(x,z) E_z^{\mathrm{SP}}(x,z)]\, dz$, and $B_s = \int_{-\infty}^{\infty} [E_z^{(s)}(x,z) H^{\mathrm{SP}}(x,z) - H^{(s)}(x,z) E_z^{\mathrm{SP}}(x,z)]\, dz$, where the field components $[H^{\mathrm{SP}}(x,z),\, E_z^{\mathrm{SP}}(x,z)]$, corresponding to an SP propagating in the negative x-direction with a unit power-flow at $x = 0$, are calculated analytically [1]. Also, $[H^{(a)}(x,z), E_z^{(a)}(x,z)]$ and $[H^{(s)}(x,z), E_z^{(s)}(x,z)]$ are the scattered field components of the combined incident field of beams A and $-$A, and of the incident beam B alone, respectively. Note that the integral over z is independent of x, provided that x corresponds to an

#167889 - $15.00 USD Received 3 May 2012; revised 11 Jun 2012; accepted 14 Jun 2012; published 22 Jun 2012

abscissa on the right side of the slit (see details in Ref. [16]).

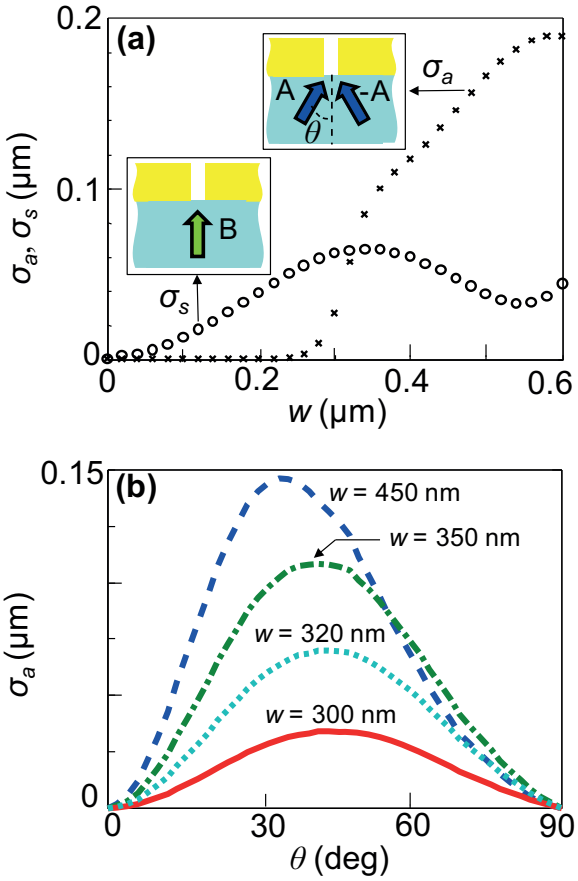

Fig. 2. The calculated SP cross sections σ_a and σ_s as defined in Eqs. (1) and (2) for a unit Poynting vector of each of the incident beams. (a) Variation of σ_a and σ_s with slit width w. The angles of incidence of the plane waves A, -A are taken to be $\theta = \pm 30^\circ$. The two insets indicate the setup for calculating σ_a and σ_s, respectively. (b) Variation of σ_a with angle of incidence θ for slit widths $w = 300, 320, 350$, and 450 nm. The refractive index of gold $n_{\mathrm{Au}} = 0.18 + \mathrm{i}2.99$ for $\lambda = 632.8$ nm, is taken from Ref. [17], and the thickness of the gold film is 200 nm.

We define

$$\sigma_s = 2|B_s|^2, \tag{1}$$

which has a dimension of length for our two-dimensional case and can be seen as a SP cross-section [18,19], by analogy with the scattering or extinction cross-sections defined for nanoparticles [20]. The factor 2 takes into account the SPs launched on both sides of the slit. The anti-symmetric case corresponds to a spatially non-uniform illumination of the slit. Usually scattering cross sections are defined for incident fields that do not vary at the scale of the scatterer. However, this Ansatz is not necessary, and in a consistent manner we may define an anti-symmetric SP cross section

$$\sigma_a = 2|A_a|^2, \tag{2}$$

#167889 - $15.00 USD Received 3 May 2012; revised 11 Jun 2012; accepted 14 Jun 2012; published 22 Jun 2012

where the integral A_a is normalized such that the Poynting-vector modulus of each individual plane wave, A and -A, is one half. On spatial averaging over the fringe pattern formed by the interference of the two incident plane waves, the total energy transported by the two-beam combination is precisely equal to the energy transported by the single plane wave B in the symmetric case. Finally, note that an SP scattering cross-section greater than the geometrical cross section of the slit (w) implies that more energy is converted to SPs than is geometrically incident upon it.

Figure 2 summarizes the main results obtained for the cross-sections at $\lambda = 632.8$ nm and for a gold-film thickness of 200 nm. In Fig. 2(a) the influence of the slit width is shown. The calculation of σ_a is performed by assuming that the angle of incidence of the plane waves with amplitude A and -A is $\theta = 30^\circ$. Starting from $w = 0$, the SP cross section of the symmetric case (circles) increases gradually to a maximum value ~ 60 nm at $w \approx 300$ nm, and then decreases as the slit width is further increased. The overall behavior is consistent with earlier works on the ability of isolated slits or grooves to launch SPs [16]. More interesting is the anti-symmetric case (crosses) for which the slit is placed at an anti-node of the interference pattern formed by the two incident plane waves. For very small slit widths, the incident field on the slit is virtually null and the TM_1 mode is weakly excited. In addition, since the TM_1 mode is below cutoff, the energy transfer towards the upper slit aperture is inefficient, and it is only when this mode becomes propagating (for $w \approx 300$ nm) that a rising behavior is observed. Then σ_a rapidly becomes significantly larger than σ_s. This remarkable result (note that the incident field is null at the slit center for the anti-symmetric case) attests to the great potential of the TM_1 mode to deliver large and steady SP flows, a property that is rarely used in plasmonic devices [21] whose operation mostly rely on the fundamental TM_0 mode and on tiny slits or grooves. [1–5, 9–13]

Figure 2(b) shows the influence of the angle θ on the SP cross section σ_a. Starting from $\theta = 0$ (a degenerate asymptotic case for which the incident field is null), the general trend is an increase of σ_a to a peak value for an intermediate angle of incidence, followed by a monotonic decrease to null for $\theta = 90^\circ$. This behavior depends only weakly on the slit width, although we note that as w increases, the angle for maximum SP excitation is gradually shifted to a less oblique angle of incidence, ranging from $46^\circ > \theta > 36^\circ$ for the range of slit widths considered from 300 nm to 450 nm. For $\theta \approx 20^\circ$ and $w = 450$ nm as used in the experiment hereafter, $\sigma_a = 100$ nm, implying that 22% of the energy directly incident onto the slit is converted into SPs launched on the upper interface.

Turning our attention back to the plasmon switch (Fig. 1), it is clear that the SP amplitudes $\beta^{(l)}$ and $\beta^{(r)}$ of the left and right traveling surface plasmons may be represented as a linear combination of the SPs excited by the TM_0 and the TM_1 mode. It follows that $\beta^{(l)}$ and $\beta^{(r)}$ are given by the expressions

$$\beta^{(l)}(\delta) = B_s e^{i\delta} + A_a, \tag{3a}$$

$$\beta^{(r)}(\delta) = B_s e^{i\delta} - A_a, \tag{3b}$$

where δ is a variable phase controlled by the voltage across the piezo element in the normally incident beam B. As will be seen shortly, the independent excitation of the two modes, together with the adjustable phase δ, allows us to control the direction in which the SPs are launched. By using variable grey filters or by varying the angle of incidence, it is possible to carefully tune the intensity of the beams to compensate for the difference between SP cross-sections σ_a and σ_s, and hence set $|B_s| = |A_a|$. In that case we have for the two SP intensities $I^{(l)}(\delta)$ and $I^{(r)}(\delta)$ the formulas

$$I^{(l)}(\delta) = |\beta^{(l)}(\delta)|^2 = 2|B_s|^2(1 + \cos\delta), \tag{4a}$$

$$I^{(r)}(\delta) = |\beta^{(r)}(\delta)|^2 = 2|B_s|^2(1 - \cos\delta). \tag{4b}$$

#167889 - $15.00 USD Received 3 May 2012; revised 11 Jun 2012; accepted 14 Jun 2012; published 22 Jun 2012

We note that a) the total plasmon intensity $I^{(l)}(\delta)+I^{(r)}(\delta)=4|B_s|^2$ is independent of the phase δ, and b) the ratio $I^{(l)}(\delta)/I^{(r)}(\delta)$ ranges from zero to infinity when δ is varied. In other words, under precise coherent illumination, a single slit supporting two propagating modes allows one to dynamically distribute a fixed surface plasmon flow between left-going SPs and right-going SPs.

We note that for wider slits, that allow more than two TM modes, one could use the same scheme to obtain plasmon steering. In such a multi-mode slit the combination of beams A and -A only excites odd modes, whereas beam B excites only even modes. Cancellation of the combined odd modes by the combined even modes at one side of the slit can be achieved by balancing the amplitudes of the beams. The SPs are then launched from the other side of the slit. However, in a wider slit the conversion of incident light into SPs will be less efficient as more light is directly transmitted.

3. Experiment

Figure 3 shows the experimental setup with which the proposed steering of the SP intensities was realized. The linearly-polarized output of a 16 mW He-Ne laser operating at $\lambda = 632.8$ nm is first divided into three beams. Each beam is passed through a combination of quarter-wave plates and a linear polarizer such that the field at the sample is TM polarized. To ensure coherent mode excitation, the path difference between the arms was minimized by use of delay lines in arms B and A. Arm B is normally incident, whereas arms A and -A are obliquely incident in air at $+30^\circ$ and -30°, respectively. By mounting the last mirror in arm -A on a micrometer linear translator the two oblique arms are made to have a π phase difference with respect to each other. The last mirror in Arm B is mounted on top of a piezo element which is connected to a DC voltage source with a range of $0-300$ V. The voltage across the piezo determines the phase δ of beam B. In a separate interference experiment with the same laser, the piezo voltage scale was calibrated in terms of phase, yielding that a 120 V ramp corresponds to a $\pi-$phase shift in δ.

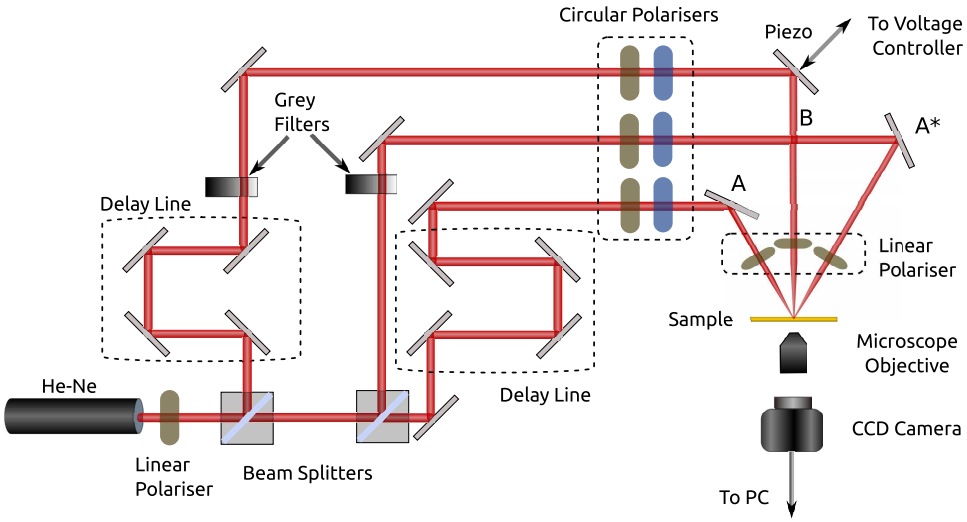

Fig. 3. Sketch of the experimental setup. The sample is illuminated from the glass-substrate side.

Scanning electron microscopy (SEM) images of the fabricated sample are shown in the insets

#167889 - $15.00 USD Received 3 May 2012; revised 11 Jun 2012; accepted 14 Jun 2012; published 22 Jun 2012

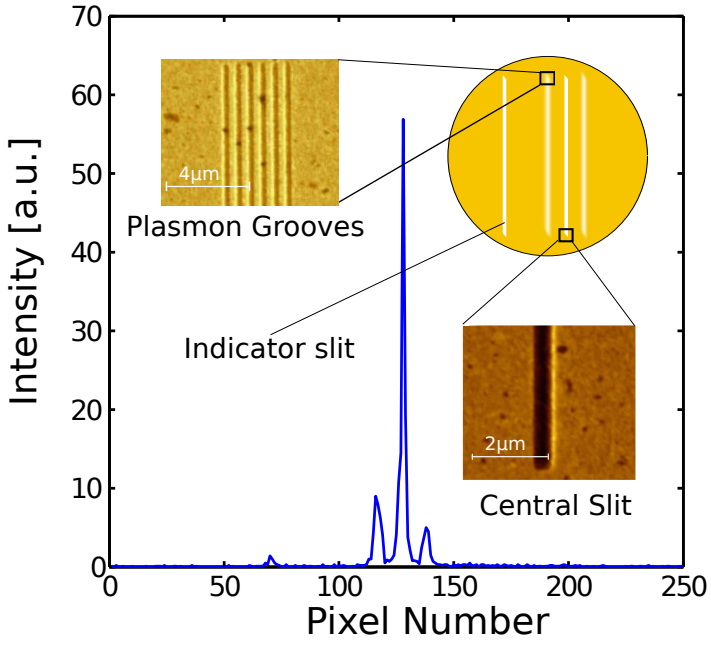

Fig. 4. Typical line trace of the CCD camera screen, perpendicular to the slits. The first low peak on the left (near pixel 70) is the signal from the indicator slit. The second and fourth peak are the intensities $I^{(l)}(\delta)$ and $I^{(r)}(\delta)$ from surface plasmons scattered by the left-hand grooves and right-hand grooves, respectively. The highest peak is the intensity transmitted by the central slit. The insets show sample details of the the central slit and the plasmon grooves made by a scanning electron microscope.

of Fig. 4. Subwavelength slits with widths varying between 250 and 650 nm were etched by electron-beam lithography followed by ion-beam etching in a 200 nm thick gold layer evaporated onto a 0.5 mm thick fused-silica substrate. On either side of this "central slit", at a distance of 8 μm, there is a set of 6 grooves with a 600 nm center-to-center spacing. Due to their tiny widths, only the central slits are etched all throughout the gold film, whereas the grooves are only partially engraved. To ease the alignment procedure, there is a reference slit located at a distance of around 25 μm to the left of each central slit. A 450 nm wide slit, which supports both the TM_0 and TM_1 modes, was used for the experimental results reported hereafter, but similar results have been obtained with other widths. The 8 μm slit-grooves separation helps suppress the amplitude of the quasi-cylindrical waves so that the grooves serve only to scatter the SPs. This ensures that the line trace pattern of the CCD camera in the far-field is effectively proportional to the intensity of the SPs and is not contaminated with additional direct-wave contributions [22].

Experimental results for the 450 nm wide slit are shown in Fig. 5, where the intensities of the left- and right-travelling surface plasmons, $I^{(l)}(\delta)$ and $I^{(r)}(\delta)$ are plotted as a function of the voltage across the piezo element that regulates the phase δ of the normally incident beam. The agreement with Eq. (4) is very good. It is seen that more than 94% of the surface plasmons are launched to the left when the piezo voltage is 80 V, whereas for a voltage of 200 V about 92% is launched to the right. For intermediate voltage settings, arbitrary ratios of $I^{(l)}(\delta)/I^{(r)}(\delta)$

#167889 - $15.00 USD Received 3 May 2012; revised 11 Jun 2012; accepted 14 Jun 2012; published 22 Jun 2012

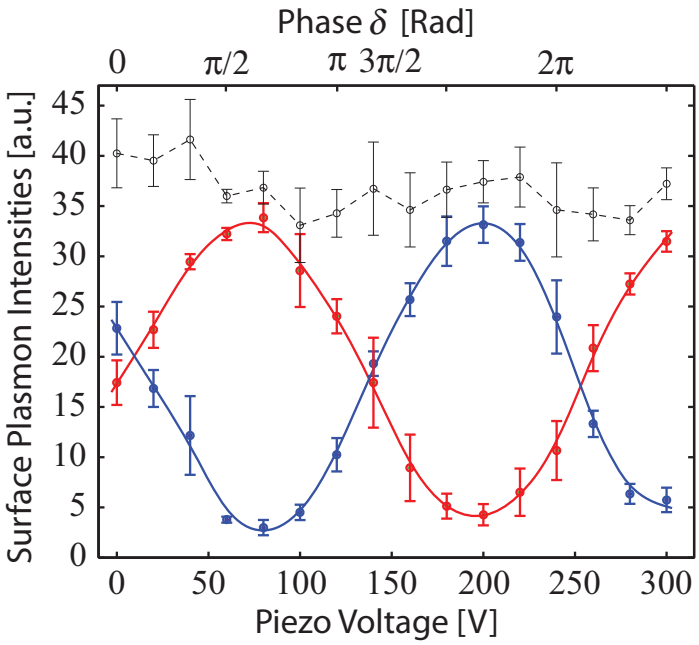

Fig. 5. Experimental results of the proposed plasmon switching method. The SP intensities $I^{(l)}(\delta)$ (red curve) and $I^{(r)}(\delta)$ (blue curve) are shown as a function of the phase δ of arm B or, equivalently, as a function of the voltage across the piezo element. The total intensity $I^{(l)}(\delta)+I^{(r)}(\delta)$ is shown as a dotted grey curve. The error bars indicate the standard deviation of ten independent measurements.

can be obtained, which makes the device act as a variable beam splitter. The average total intensity $I^{(l)}(\delta)+I^{(r)}(\delta)=36.6$ (dotted grey line). The attained visibility of 0.82 is limited by several factors, viz. a) the three beams not being spatially fully coherent due to the relatively low coherence length of the He-Ne laser, b) the amplitudes of arms A and -A being different by about $2-4\%$, and c) the amplitude $|B_s|$ differing from $|A_a|$ by about $2-5\%$. Notice however, that the sum of the two SP intensities is rather constant, with a mean value of 36.6 and a relative standard deviation less than 7% over the entire voltage sweep. Also the peak to minimum distance of 120 V is in excellent agreement with the independently observed π change in the phase δ of arm B. Additionally, by performing far-field measurements of the intensity radiated by the slit, we have observed a "lighthouse effect", i.e. the maximum in the far-field intensity distribution can be continuously shifted from the left to the right and vice versa, as one varies the voltage across the piezo element. This suggests that one may also achieve beam steering in the far-field of a two-mode nanoslit by controlling the linear combination of the two modes.

4. Conclusion

In conclusion, we have demonstrated that the selective coherent excitation of the two fundamental TM modes in a sub-wavelength slit allows us to launch an approximately constant intensity of surface plasmons either to the left or to the right of the slit; or to distribute them in any desired ratio over these two directions. This gives, for the first time, dynamic control over the directionality of surface plasmons. Our theoretical analysis shows that, although its excitation requires a null illumination at the slit center, the TM_1 mode above cutoff offers the potential of

#167889 - $15.00 USD Received 3 May 2012; revised 11 Jun 2012; accepted 14 Jun 2012; published 22 Jun 2012

higher SP conversion efficiencies compared to narrow sub-wavelength apertures that support only the TM_0 mode. Note that the radially polarized TM_{01} mode of subwavelength circular holes [23] presents an axial field singularity and is likely, just as the TM_1 mode of slits, to efficiently generate SPs.

The present work illustrates how the combination of a static symmetric structure with a versatile illumination scheme may lead to the controlled launching of surface or guided waves at the nanoscale, and as such it may be considered as a generic demonstration. Indeed, further work is needed to realize a competitive device. With additional calculations, we have checked for $\lambda = 0.6\ \mu$m that as high as 40% and 55% of the TM_0 and TM_1 modes are scattered into SPs at the slit exit aperture. Therefore, the throughput of our experimental system is presently limited by the coupling between the incident beams and the slit modes. This coupling can be further improved by increasing either the refractive index of the substrate, or the cross-section of the slit aperture. Different approaches that preserve the symmetry are possible, for example surrounding the slit with an array of optimized phased grooves [13, 24, 25], or placing a nano-antenna at the near-field of the slit entrance [26]. This would keep the transverse size of the switching device below the diffraction limit. A drastic miniaturization of our table-top illumination setup can be achieved with micro-optical components and gratings, and thanks to the very fast development of active plasmonics technologies [27], it would be interesting to investigate architectures for full on-chip integration. Such an ultra-compact plasmonic switch would have potential application in telecommunications and optical sensing.

Acknowledgments

The authors wish to thank Jacques Bouma for his technical assistance, and Jean-Paul Hugonin for helpful discussions. The sample was fabricated at the IOGS-TRT nanofabrication platform. S.B.R. is supported by the Dutch Technology Foundation (STW). T.D.V. acknowledges support from the Plasmonics program of the Foundation for Fundamental Research on Matter (FOM).

#167889 - $15.00 USD Received 3 May 2012; revised 11 Jun 2012; accepted 14 Jun 2012; published 22 Jun 2012